Electronic Supplementary Material (ESI) for Physical Chemistry Chemical Physics.

Supporting information:

Accurate thermodynamic properties of gas phase hydrogen bonded complexes

Anne S. Hansen, Zeina Maroun, Kasper Mackeprang, Benjamin N. Frandsen, and Henrik G. Kjaergaard*

Department of Chemistry, University of Copenhagen, Universitetsparken 5, DK-2100 Copenhagen Ø, Denmark

E-mail: hgk@chem.ku.dk

Phone: +45-35320334. Fax: +45-35320322

---

*To whom correspondence should be addressed

S1 Experimental details and validation

Three identical experiments of the EtOH·DMA complex were performed (Figures 3, S1 and S2), in which the initial pressures of EtOH and DMA were within 1 Torr of each other (13.4 Torr EtOH + 18.7 Torr DMA, 14.0 Torr EtOH + 19.4 Torr DMA, and 13.6 Torr EtOH + 19.5 Torr DMA referred to as experiment 1, 2, and 3, respectively). Two experiments of the MeOH·DMA complex were performed (Figure 3 and S3), which are referred to as experiment 4 and 5. In each experiment, nine measurements at different temperatures were performed, each recored with 500 scans. The temperature and the pressure were noted at every 50 scan. An average of the 10 noted pressures and temperatures was used as the pressure and temperature for that measurement. Experimental details for experiments 1 - 5 are given in Tables S1 - S5. Examples of the integrated absorbance for each complex are given in Figure S4.

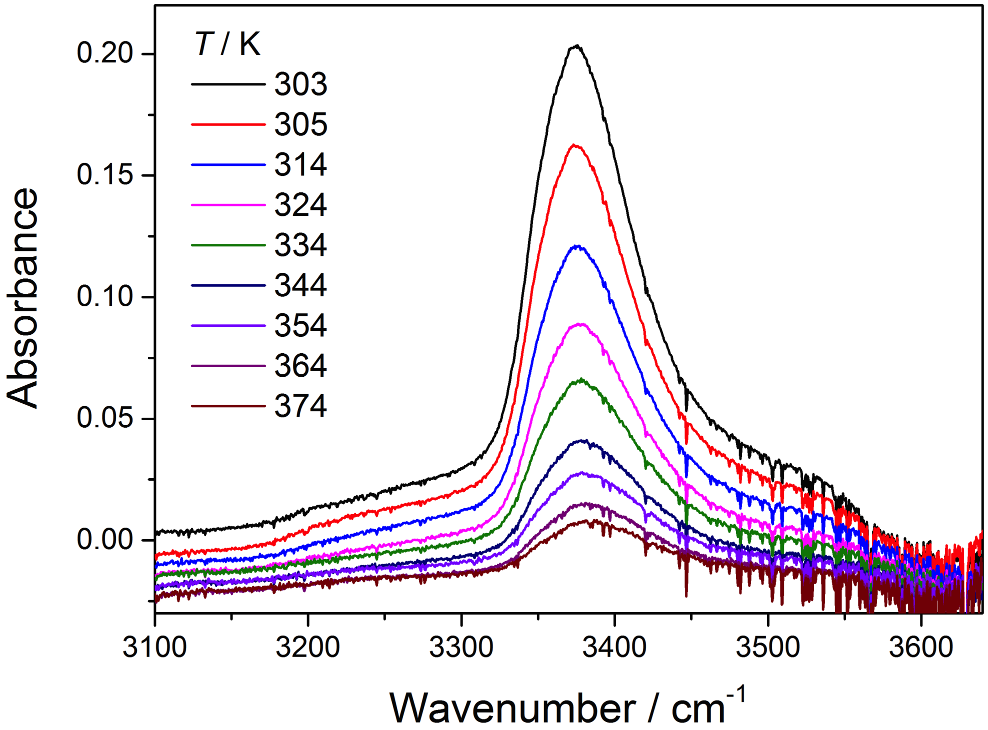

Figure S1: The OH-stretching vibration in the EtOH·DMA complex, recorded at different temperatures, experiment 2, Table S2.

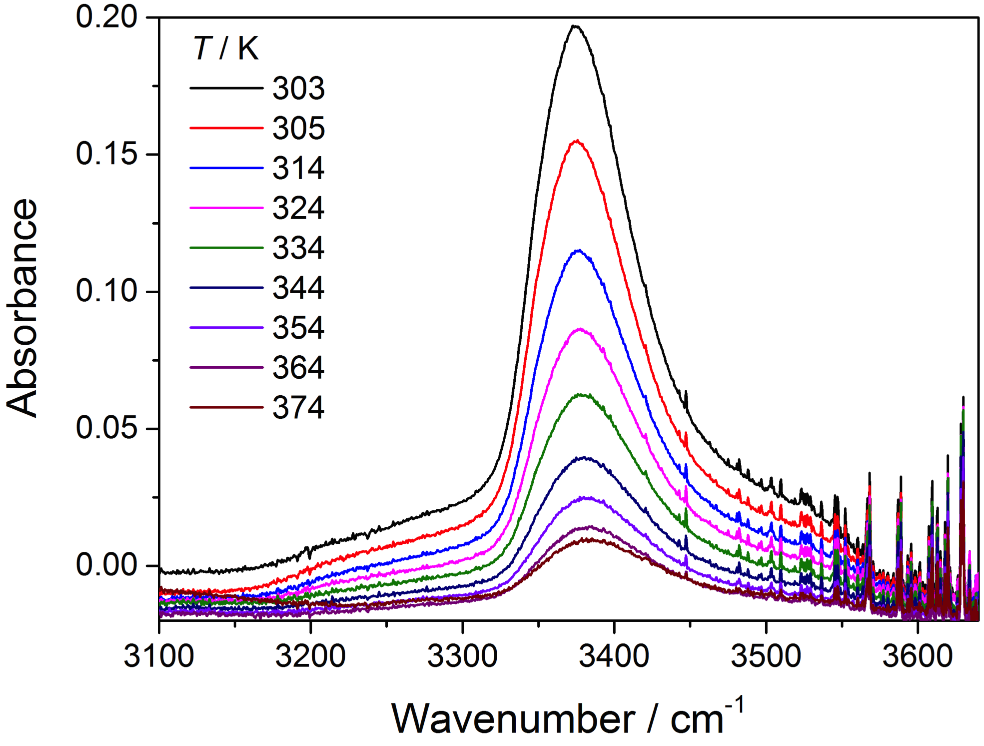

Figure S2: The OH-stretching vibration in the EtOH·DMA complex, recorded at different temperatures, experiment 3, Table S3.

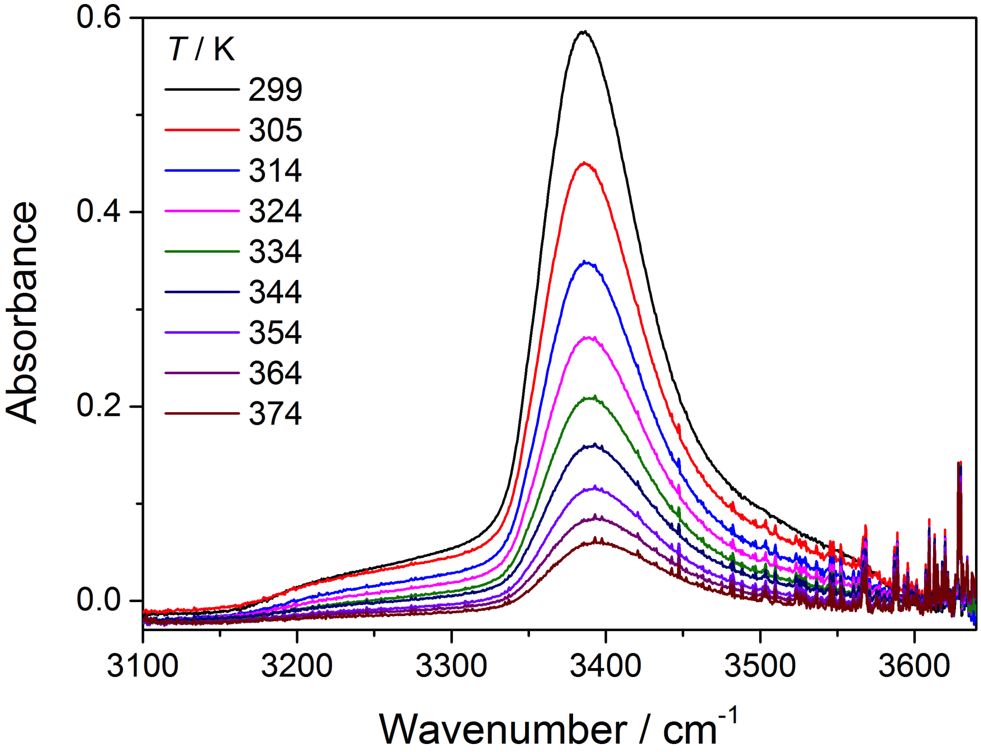

Figure S3: The OH-stretching vibration in the MeOH·DMA complex, recorded at different temperatures, experiment 2. The temperatures given are the average temperatures.

Table S1: Experimental data for experiment 1. The average temperatures (K), EtOH and DMA average pressures (Torr) in the experiments, the integrated absorbance (cm^{-1}) of the observed OH-stretching band and the OH-stretching frequency ($\tilde{\nu}_{\mathrm{max}}$, in cm^{-1}) at the maximum absorbance (A_{max}).

Mix.	T^{a}	P_{EtOH}	P_{DMA}	Int. Abs	$\tilde{\nu}_{\mathrm{max}}$	A_{max}
A	301	13.4	18.7	25.6	3374	0.203
B	305	14.0	19.8	20.1	3375	0.161
C	314	16.0	21.1	17.1	3376	0.127
D	324	17.1	22.2	12.8	3377	0.098
E	334	18.1	23.2	10.2	3378	0.076
F	344	19.2	24.0	7.76	3379	0.059
G	354	20.1	24.7	6.09	3380	0.046
H	364	21.0	25.4	4.47	3381	0.035
I	374	22.0	26.0	2.81	3384	0.024

a: An average of the 10 noted temperatures during a measurement of 500 scans, *vide supra*.

Table S2: Experimental data for experiment 2, where the measurements were started after the temperature had equilibriated. The average temperatures (K), EtOH and DMA average pressures (Torr) in the experiments, the integrated absorbance (cm^{-1}) of the observed OH-stretching band and the OH-stretching frequency ($\tilde{\nu}_{\text{max}}$, in cm^{-1}) at the maximum absorbance (A_{max}).

Mix.	T	P_{EtOH}	P_{DMA}	Int. Abs	$\tilde{\nu}_{\text{max}}$	A_{max}
A	303	14.0	19.4	23.4	3374	0.204
B	305	13.5	19.9	19.5	3375	0.167
C	314	15.0	21.1	16.0	3376	0.132
D	324	16.2	22.0	12.7	3377	0.103
E	334	17.0	22.9	9.40	3378	0.081
F	344	17.9	23.6	7.01	3379	0.059
G	354	18.5	24.3	5.78	3380	0.046
H	364	19.8	25.1	4.58	3381	0.037
I	374	20.7	25.7	3.49	3384	0.027

Table S3: Experimental data for experiment 3, where the measurements were started after the temperature had equilibriated. The average temperatures (K), EtOH and DMA average pressures (Torr) in the experiments, the integrated absorbance (cm^{-1}) of the observed OH-stretching band and the OH-stretching frequency ($\tilde{\nu}_{\text{max}}$, in cm^{-1}) at the maximum absorbance (A_{max}).

Mix.	T	P_{EtOH}	P_{DMA}	Int. Abs	$\tilde{\nu}_{\text{max}}$	A_{max}
A	303	13.6	19.5	23.5	3374	0.201
B	305	13.5	19.6	19.5	3375	0.176
C	314	14.8	20.8	15.6	3376	0.137
D	324	15.7	21.7	12.1	3377	0.106
E	334	16.5	22.4	9.93	3378	0.081
F	344	17.3	23.5	7.55	3379	0.062
G	354	18.1	24.1	5.57	3380	0.046
H	364	19.1	24.7	4.53	3381	0.036
I	374	19.9	24.9	3.22	3384	0.028

Table S4: Experimental data for experiment 4. The average temperatures (K), MeOH and DMA average pressures (Torr) in the experiments, the integrated absorbance (cm^{-1}) of the observed OH-stretching band and the OH-stretching frequency ($\tilde{\nu}_{\max}$, in cm^{-1}) at the maximum absorbance ($A_{\max}$).

Mix.	T	P_{MeOH}	P_{DMA}	Int. Abs	$\tilde{\nu}_{\max}$	$A_{\max}$
A	301	15.6	20.3	29.9	3386	0.280
B	305	14.8	20.1	23.7	3387	0.214
C	314	15.5	21.0	18.1	3388	0.164
D	324	16.1	21.8	14.3	3389	0.127
E	334	16.6	22.5	10.8	3390	0.096
F	344	17.0	23.5	8.41	3391	0.076
G	354	17.9	24.0	6.73	3392	0.059
H	364	18.6	24.7	5.01	3393	0.045
I	374	18.9	25.5	2.90	3394	0.030

Table S5: Experimental data for experiment 5. The average temperatures (K), MeOH and DMA average pressures (Torr) in the experiments, the integrated absorbance (cm^{-1}) of the observed OH-stretching band and the OH-stretching frequency ($\tilde{\nu}_{\max}$, in cm^{-1}) at the maximum absorbance ($A_{\max}$).

Mix.	T	P_{MeOH}	P_{DMA}	Int. Abs	$\tilde{\nu}_{\max}$	$A_{\max}$
A	299	19.1	27.0	66.5	3386	0.595
B	305	20.6	26.4	50.1	3387	0.449
C	314	21.5	27.2	40.2	3388	0.355
D	324	22.3	28.3	31.3	3389	0.277
E	334	23.2	29.6	25.5	3390	0.219
F	344	24.0	30.6	19.1	3391	0.167
G	354	25.1	31.8	15.2	3392	0.128
H	364	25.9	32.8	11.8	3393	0.102
I	374	26.9	33.9	8.19	3394	0.072

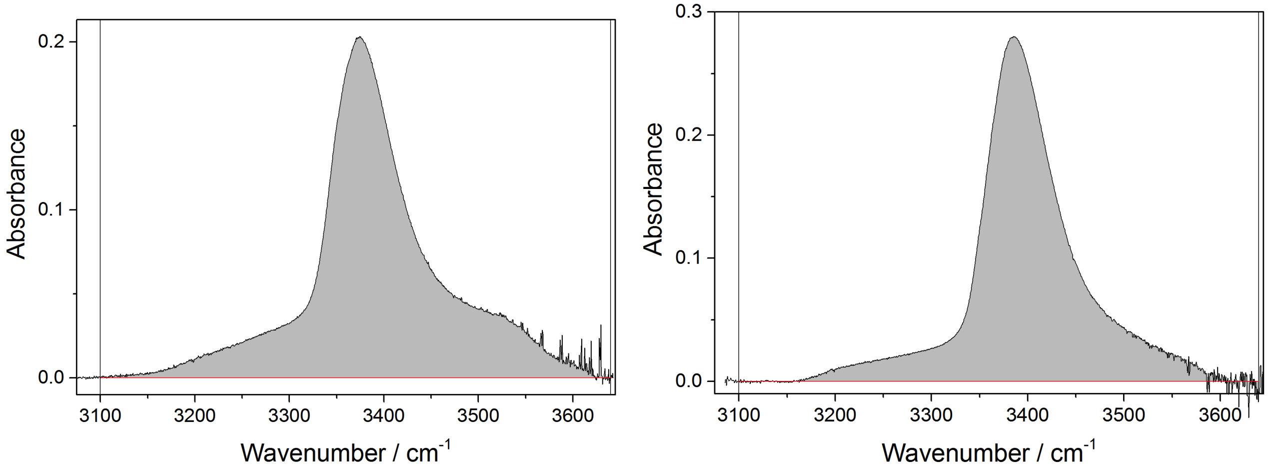

(a) (b)

Figure S4: The integrated absorbance of the OH-stretching band obtained with integration boundaries of 3100 - 3640 cm^{-1} for the EtOH·DMA (a) and MeOH·DMA (b) complexes.

S1.1 Uncertainties

S1.1.1 Equilibrium constant

K_P is determined by plotting P_{AB} as a function of $P_{\text{A}}P_{\text{B}}$, equation 5. P_{AB} corresponds to P_{C} in the manuscript. The uncertainty of K_P mainly stems from the uncertainties of P_{AB}, which arise from uncertainties in the temperature (T), the integrated absorbance ($\int A(\tilde{\nu})\, d\tilde{\nu}$) and the calculated oscillator strength (f_{calc}), equation 6. In Table S6, we summarise the uncertainties of these parameters. A total error of 17 % is obtained for P_{AB}.

Table S6: The uncertainty (in %) of the temperature (T), the integrated absorbance ($\int A(\tilde{\nu})\, d\tilde{\nu}$), the calculated oscillator strength (f_{calc}) and the monomer pressures (P_{A} and P_{B}).

T	$\int A(\tilde{\nu})\, d\tilde{\nu}$	$f_{\text{calc}}{}^{\text{a}}$	P_{A} and P_{B}	A_{Max}
2	5	10	10	5

a: LMPT calculated f of the OH-stretching vibration.

Error bars are included in the plot of P_{AB} against $P_{\text{A}}P_{\text{B}}$. A straight line is fitted to the data points using the linear least squares fit, where the error bars have been weighted. This is done with the OriginPro 2015 software using the instrumental weighting.

S1.1.2 Enthalpy

ΔH is determined by plotting $\ln K_P$ *versus* T^{-1}. K_P is obtained from equation S4, and the uncertainty of ΔH stems from uncertainty in the temperature (T), the integrated absorbance ($\int A(\tilde{\nu})\,d\tilde{\nu}$) and the monomer pressures (P_A and P_B), which are summarised in Table S6. A total error of 27 % is obtained for T, $\int A(\tilde{\nu})\,d\tilde{\nu}$, P_A and P_B. Error bars are included in the plot of $\ln K_P$ against T^{-1}.

S1.2 Temperature and pressure fluctuations

To test the pressure and temperature variation during a measurement, the temperature and the pressure were noted at every 50 scan. An average of the 10 noted pressures and temperatures was used to determine the given pressure and temperature for each measurement. In Figure S5, the temperature and pressure variation during a measurement of 500 scans is shown. Nine measurements of an EtOH + DMA mixture in the room temperature (RT) - 373 K temperature range are shown. The cell temperature and pressure were read every 50 scans (every ∼20 seconds) for each of the nine measurements.

The temperature controller was set to a certain temperature (T_set); however, the actual cell temperature would initially reach a temperature 4 - 7 K higher than T_set and thereafter cool to 1 - 2 K lower than T_set, only to rise again to 4 - 7 K higher than T_set and so on. Once the cell temperature had increased to its maximum value and subsequently fallen to its minimum value, one temperature cycle was completed. We refer to the temperature as equilibrated after one cycle. When T_set was 303 K, it took approximately 20 minutes for the temperature to drop from its maximum to minimum value, whereas it took only approximately 2 minutes when T_set was 373 K. A single measurement with 500 scans and a 1 cm^{-1} resolution took 3.5 minutes and thus at small T_set values, the temperature was almost constant in the course of a measurement, Figure S5a. At high T_{set} values, the cell temperature dropped and subsequently rose ∼6 K in the course of a measurement. As a test, we recorded spectra at $T_{\mathrm{set}} = 303$ K before and after the temperature had equilibrated. The spectra were similar and the average temperatures in the experiment before and after equilibration were 309 K and 305 K, respectively. Hence, the starting time of a measurement has little effect on the resulting spectra, average temperatures, measured pressures (max variation of 0.7 Torr) and determined equilibrium constants.

In Figure S5b, the pressure fluctuations in the cell are shown. The pressure is almost constant throughout the measurements, with a variation of ±1 Torr in the course of a measurement. This trend is observed for all measurements, except the room temperature (brown stars) measurement. Here, the pressure continuously drops, probably due to condensation of EtOH onto the cell walls. Consequently, the pressure measured at 303 K (purple dots) is lower than the initial pressure at room temperature.

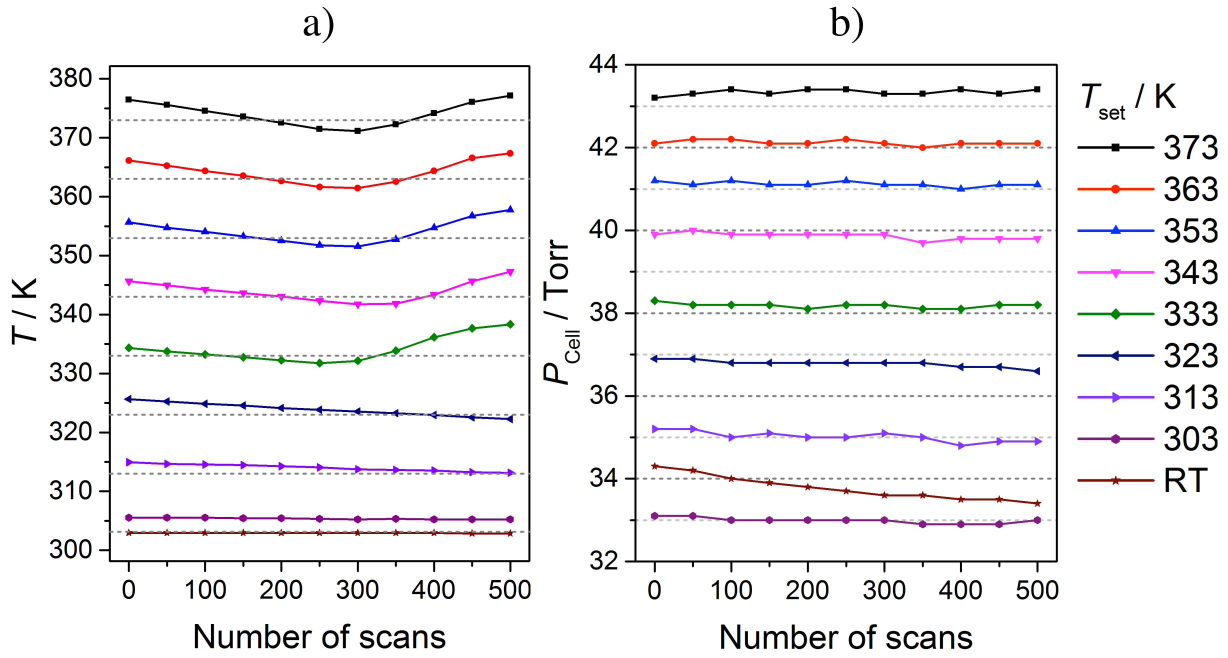

Figure S5: Measurement of an EtOH + DMA mixture at different temperatures. The corresponding average temperatures and EtOH and DMA pressures are given in Table S3. The T_{set} value is the temperature set on the temperature controller, and RT refers to the room temperature measurements before the heating jacket has been turned on. The actual measured temperatures are given Table S3. The temperature (a) and pressure (b) variations in the cell in during a measurement.

S1.3 Determination of pressures with the ideal gas law

We measure the pressure in the cell during all experiments in the room temperature (299 - 303 K) to 373 K range. We can estimate the pressures at elevated temperatures from the pressure measured at room temperature and the ideal gas law:

$$\frac{P_{\text{RT}}V}{P_{\text{x}}V} = \frac{nRT_{\text{RT}}}{nRT_{\text{x}}} \Leftrightarrow P_{\text{x}} = P_{\text{RT}}\frac{T_{\text{x}}}{T_{\text{RT}}}, \tag{S1}$$

where P_{x} is the pressure at elevated temperatures, P_{RT} is the pressure measured at room temperature, T_{RT} is the room temperature and T_{x} is the measured elevated temperature. P_{RT} is the initial pressure measured (0 - 50 scans, Figures S5b), as we assume the alcohol that condensates on the cell wall will re-evaporate at elevated temperatures. If we compare the calculated ideal gas law pressure with the pressure measured in the experiment, we obtain an indication of the accuracy of the calculated ideal gas law pressure. In Figure S6, we compare the measured and calculated pressures of EtOH and DMA in a measurement of an EtOH + DMA mixture. The measured EtOH and DMA pressures are obtained from spectral subtraction,[1–7] where the individual scaled monomer spectra are subtracted from the EtOH + DMA mixture. The experimental details are summarised in Table S1. Eight measurements were performed at different temperatures (B - I), where B and I are $T_{\text{set}} = 303$ K and 373 K temperature measurements, respectively. The room temperature measurement (A) is not included in the figure, as the ideal gas law was not used to calculate the pressures at this temperature.

At all temperatures, the pressure calculated with the ideal gas law is lower than the measured pressure (3 - 32 %). As the temperature increases (B → I), the discrepancy between the calculated and measured pressures increases. We also find that the calculated EtOH pressure is underestimated more than the calculated DMA pressure. At $T_{\text{set}} = 373$ K the EtOH and DMA ideal gas law pressures are underestimated by 32 % and 12 %, respectively. Sample condensation was observed in the room temperature measurements, Figure S5b, which we assume re-evaporates from the cell wall at elevated temperatures. In the calculated ideal gas law pressures, the re-evaporation is not taken into account, and the pressures calculated at the elevated temperatures are underestimated. EtOH condensates more than DMA, which explains why the calculated EtOH pressure is underestimated more than the DMA pressure. In equation S1, we assume that the number of molecules is constant as the temperature is changed. However, as the temperature increases the number of molecules increases, as the hydrogen bound complex is broken (AB → A + B). This effect causes an overestimation of the calculated ideal gas law pressure. We expect the changes in the number of molecules to be small in the 300 - 373 K range, and the deviation observed between the measured and calculated pressures is believed to arise from sample condensation.

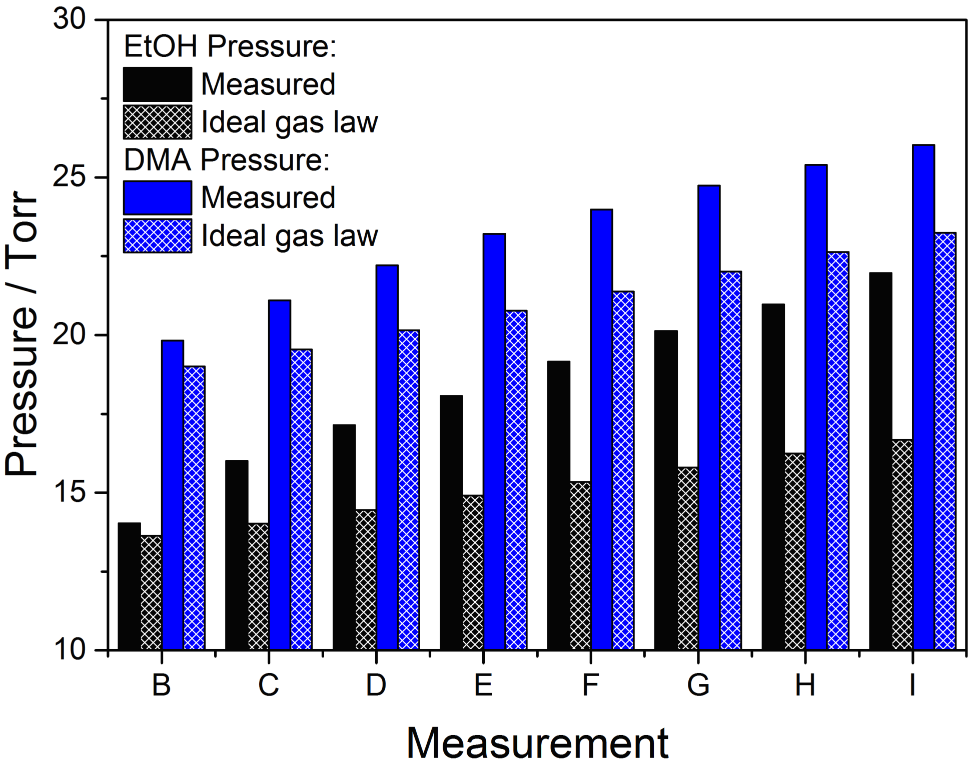

Figure S6: EtOH and DMA pressures in an EtOH + DMA mixture. The measured pressure and the calculated ideal gas law pressure are compared. Eight temperature experiments were performed, referred to as B - I, where B and I are the 303 K and 373 K temperature measurements, respectively. The room temperature experiment is not included in the figure, as it is not calculated with the ideal gas law. The experimental data corresponds to that given in Table S1.

In Figures S7 and S8, similar pressure plots are shown for the additional EtOH·DMA measurements and the MeOH·DMA measurements, respectively. In the EtOH·DMA experiments, similar trends are observed between the measured and ideal gas law pressures. Compared to the measured pressure, the EtOH and DMA ideal gas law pressures in the 313 - 373 K range are underestimated by 3 - 20 % and 3 - 7 %, respectively. However, in experiment B (303 K) the EtOH and DMA pressures predicted by the ideal gas law are slightly larger than the measured values, 1 - 5 %.

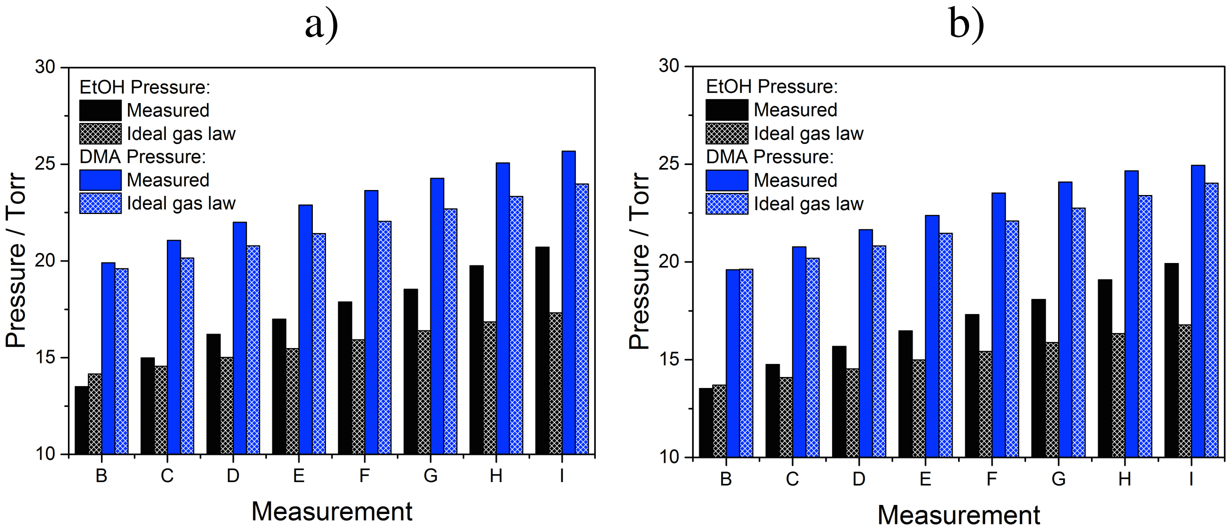

Figure S7: Comparison the measured pressure and the calculated ideal gas law pressure as in Figure S6. Part a and b of the figure corresponds to experiments 2 and 3, respectively, see Tables S2 and S3.

For the high pressure experiment of the MeOH·DMA complex, Figure S8b, good agreement is found between the calculated and measured DMA pressure, with a difference of only 1 - 4 %. Compared to the measured pressure, the MeOH ideal gas law pressures in the 313 - 373 K range are underestimated by 5 - 12 %, which is similar to the difference found for the EtOH pressure. In the other MeOH·DMA measurement, Figure S8a, small differences are found between the calculated and measured MeOH and DMA pressures. The ideal gas law MeOH pressure is overestimated by 1 - 6 % compared to the measured pressure in the 313 - 373 K range. The good agreement between the calculated and measured MeOH pressure is probably due to the low MeOH pressure used, which causes less condensation. The difference between the measured and calculated DMA pressures is smaller than 2 %. However, in general the ideal gas law estimates pressures that are 1 - 32 % from the actual measured pressures, and we recommend that the sample cell should always be equipped with a pressure gauge.

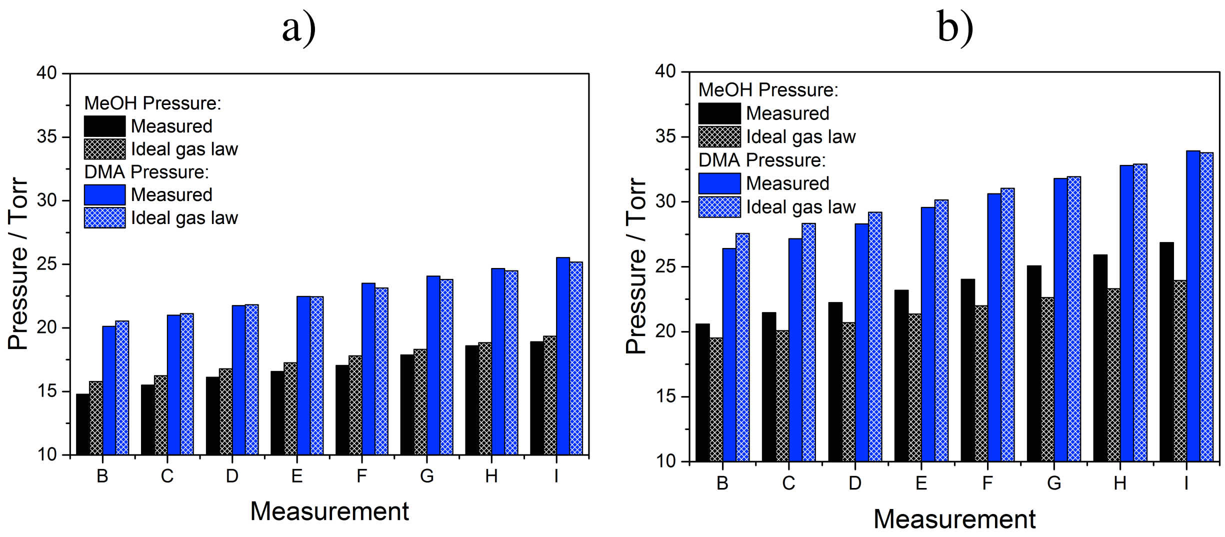

Figure S8: Comparison the measured pressure and the calculated ideal gas law pressure are compared as in Figure S6. Part a and b of the figure correspond to experiments 1 and 2, respectively, see Tables S4 and S5.

S2 Equations

The equlibrium constant, K_P, of the complex formation is given by:

$$K_P = \frac{P_{\mathrm{AB}}/P^{\ominus}}{P_{\mathrm{A}}/P^{\ominus} P_{\mathrm{B}}/P^{\ominus}}. \tag{S2}$$

If we insert the expression:

$$P_{\mathrm{AB}} = 2.6935 \times 10^{-9}[\mathrm{K}^{-1}\ \mathrm{Torr\ m\ cm}] \frac{T \int A(\tilde{\nu})\, d\tilde{\nu}}{f_{\mathrm{calc}}\ l}, \tag{S3}$$

used to determine the pressure of the complex, we can write K_P as:

$$\begin{aligned} K_P &= 2.6935 \times 10^{-9}[\mathrm{K}^{-1}\ \mathrm{Torr\ m\ cm}] \frac{T \int A(\tilde{\nu})\, d\tilde{\nu}/P^{\ominus}}{f_{\mathrm{calc}}\ l\ P_{\mathrm{A}}/P^{\ominus} P_{\mathrm{B}}/P^{\ominus}} && \text{(S4)} \\ &= F \times \frac{T \int A(\tilde{\nu})\, d\tilde{\nu}}{P_{\mathrm{A}}/P^{\ominus} P_{\mathrm{B}}/P^{\ominus}}, && \text{(S5)} \end{aligned}$$

where the $F = 2.6935 \times 10^{-9}[\mathrm{K}^{-1}\ \mathrm{Torr\ m\ cm}]/(P^{\ominus} f_{\mathrm{calc}} l)$. If we take the natural logarithm we obtain:

$$\begin{aligned} \ln(K_P) &= \ln\Big(F \times \frac{T \int A(\tilde{\nu})\, d\tilde{\nu}}{P_{\mathrm{A}}/P^{\ominus} P_{\mathrm{B}}/P^{\ominus}}\Big) \\ &= \ln\Big(\frac{T \int A(\tilde{\nu})\, d\tilde{\nu}}{P_{\mathrm{A}}/P^{\ominus} P_{\mathrm{B}}/P^{\ominus}}\Big) + \ln\Big(F\Big). && \text{(S6)} \end{aligned}$$

We can equate this expression for $\ln(K_P)$ with the expression in equation 3 and get:

$$\ln\Big(\frac{T \int A(\tilde{\nu})\, d\tilde{\nu}}{P_{\mathrm{A}}/P^{\ominus} P_{\mathrm{B}}/P^{\ominus}}\Big) = -\frac{\Delta H}{R}\frac{1}{T} + \frac{\Delta S}{R} - \ln\Big(F\Big). \tag{S7}$$

If we assume that the bandshape does not change with temperature, we can replace the integrated absorbance with the maximum absorbance times a constant ($A_{\mathrm{max}} = \int A(\tilde{\nu})\, d\tilde{\nu} \times Y$). Thus a plot of $\ln\left(\frac{TA_{\mathrm{max}}}{P_{\mathrm{A}}P_{\mathrm{B}}}\right)$ *versus* T^{-1} would also give a straight line with $-\Delta H/R$ as the slope.

S3 Optimised structures

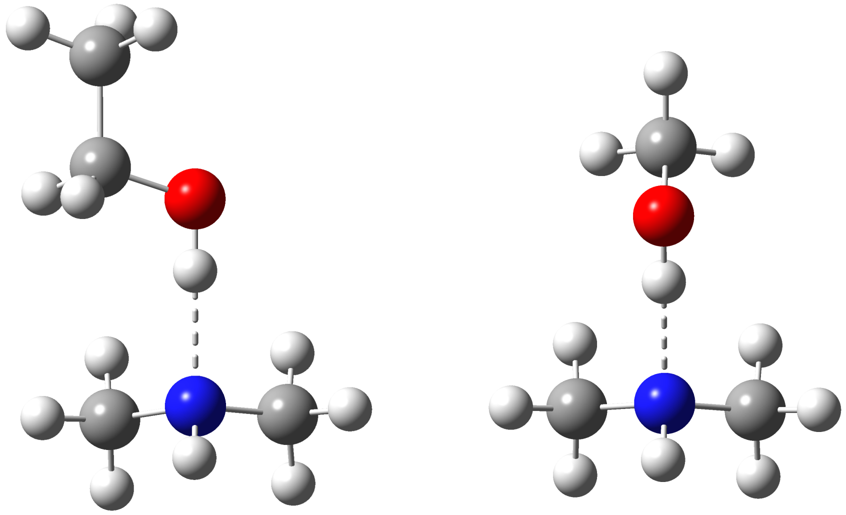

EtOH·DMA MeOH·DMA

Figure S9: CCSD(T)-F12a/VDZ-F12 optimised structures of the higher energy EtOH·DMA and MeOH·DMA conformers, with binding energies of -33.9 kJ/mol and -33.4 kJ/mol, respectively. The MeOH·DMA conformer has a small imaginary frequency of 9i cm^{-1}; however this structure was used in a previous study of the MeOH·DMA complex.[4]

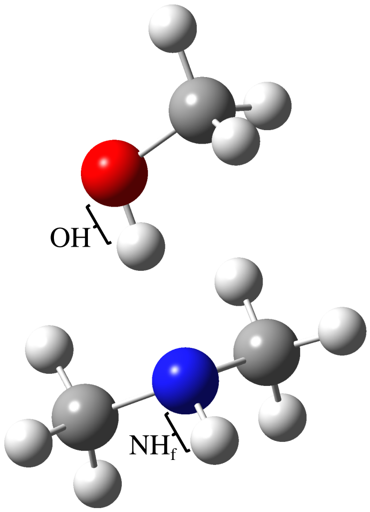

Figure S10: Illustration of the bound OH-stretching vibration and the free NH_f-stretching vibration in the MeOH·DMA complex.

S4 Calculated oscillator strengths

Oscillator strengths were calculated with a modified version of the LMPT model, which was developed to describe the donor vibrations of hydrated complexes with water as the donor unit.[8,9] The LMPT model is based on a three dimensional (3D) LM model[10] for the donor water unit and each of the six intermolecular modes is included as a one dimensional (1D) oscillator. The effect of the intermolecular modes on the donor vibrational modes is included by Rayleigh-Schrödinger perturbation theory, where each intermolecular mode couples to each of the donor vibrational modes through the potential energy surface. Kinetic energy couplings are expected to be negligible.[9] Perturbative corrections are obtained up to the fourth order in the energy and first order in the wavefunctions.[8,9]

In its modified version, the LMPT model is based on a two dimensional (2D) LM model of the OH-stretching oscillator and the COH-bending mode. The displacement coordinates of the two modes are q_b and θ, respectively. The Hamiltonian operator for this 2D system is:

$$\hat{H}_{2\mathrm{D}} = -\frac{\hbar^2}{2} \sum_{ij=q_\mathrm{b},\theta} \frac{\partial}{\partial q_i} g_{ij} \frac{\partial}{\partial q_j} + V(q_\mathrm{b}) + V(\theta) + V(q_\mathrm{b}, \theta). \tag{S8}$$

The g-matrix elements, g_{ij}, are given by:[11]

$$g_{q_\mathrm{b}q_\mathrm{b}} = \frac{1}{m_\mathrm{O}} + \frac{1}{m_\mathrm{H}} \tag{S9}$$

$$g_{\theta\theta} = \left(\frac{1}{m_\mathrm{O}} + \frac{1}{m_\mathrm{Donor} - m_\mathrm{O} - m_\mathrm{H}}\right)\frac{1}{r_\mathrm{OC}^2} + \left(\frac{1}{m_\mathrm{O}} + \frac{1}{m_\mathrm{H}}\right)\frac{1}{r_\mathrm{OH}^2} - 2\frac{\cos\phi_\mathrm{COH}}{m_\mathrm{O} r_\mathrm{OC} r_\mathrm{OH}} \tag{S10}$$

$$g_{q_\mathrm{b}\theta} = g_{\theta q_\mathrm{b}} = -\frac{\sin\theta}{m_\mathrm{O} r_\mathrm{OC}}, \tag{S11}$$

where m_{O}, m_{H} and m_{Donor} are the masses of the O atom, H atom and donor unit, respectively, and r_{OH} and r_{OC} are the OH bond length and OC bond length, respectively, and ϕ_{COH} is the COH angle. The 1D potentials, $V(q_{\mathrm{b}})$ and $V(\theta)$, are represented by spline fits. The points needed to generate the spline fit for the OH-stretch were obtained by displacing the OH bond by -0.40 Å to +0.70 Å in steps of 0.05 Å from the equilibrium structure. For the COH-bending oscillator the points needed for the spline fit were generated by displacing the COH angle by -50 degrees to +80 degrees in the steps of 5 degrees. The 2D potential energy surface, $V(q_{\mathrm{b}}, \theta)$, consist of quadratic, cubic and quartic coupling terms. The coefficients of the coupling terms have been calculated using a standard numerical technique from a 9×9 potential energy grid obtained by simultaneously displacing along the OH-stretch and COH-bend.[8,9] The displacements in this case was from -0.20 Å to +0.20 Å in steps of 0.05 Å for the OH-stretch, and from -20 degrees to +20 degrees in steps of 5 degrees for the COH-bend. A 1D Schrödinger equation was set up for each of the two donor vibrations and solved using the method described by Meyer.[12] For this purpose, the g-matrix elements at the equilibrium geometry was used. The product of the eigenfunctions obtained by solving these 1D Schrödinger equations was used as a basis to set up a vibrational Hamiltonian for the 2D system. The vibrational states and energy levels were determined by diagonalising the Hamiltonian using the matrix diagonalisation procedure in the *Matlab* software.

Previously, it has been found that two of the six intermolecular modes were the major contributors in a series of hydrated complexes, as the contribution from these two modes constituted more than 65 % of the total correction to the transition frequency in the hydrated complexes tested.[9] These two modes are the donor rock, β, and the donor twist, x, and only these two modes are included in the modified LMPT model. We employ a similar definition of the donor rock compared to the studies on the hydrated complexes,[8,9] as we define the donor rock as the CON-bending motion. However, we define the donor twist, as the rotation of the donor unit around the CO bond. This is a different definition compared to the hydrated complexes,[8,9] where the donor twist was defined as the rotation around the HOH bisecting vector of the donor water unit. Illustrations of the donor rock and twist are given in Figure S11.

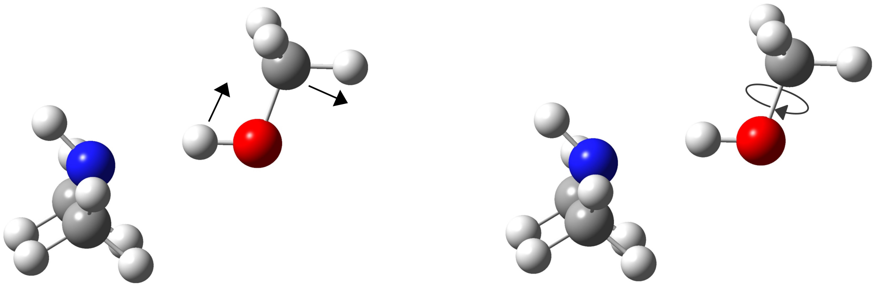
(a) Rock (b) Twist

Figure S11: Illustrations of the the donor rock (a) and the donor twist (b).

These two modes are treated as harmonic oscillators, and the harmonic frequency is determined via the second derivative of 1D potential energy surfaces obtained by displacing each intermolecular mode by -20 degrees to +20 degrees in the steps of 5 degrees. The g-matrix element of the donor rock is given by:[8,9]

$$\begin{aligned} g_{\beta\beta} =& \frac{1}{4}\left[\left(\frac{1}{m_{\mathrm{H}}}+\frac{1}{m_{\mathrm{O}}}\right)\frac{1}{r_{\mathrm{OH}}^2}+\left(\frac{1}{m_{\mathrm{Donor}}-m_{\mathrm{O}}-m_{\mathrm{H}}}+\frac{1}{m_{\mathrm{O}}}\right)\frac{1}{r_{\mathrm{OC}}^2}\right] \\ &+\left(\frac{1}{m_{\mathrm{Acceptor}}}+\frac{1}{m_{\mathrm{O}}}\right)\frac{1}{r_{\mathrm{ON}}^2}+\frac{1}{m_{\mathrm{O}}}\left(\frac{\cos\phi_{\mathrm{COH}}}{2r_{\mathrm{OH}}r_{\mathrm{OC}}}-\frac{\cos\phi_{\mathrm{NOH}}}{r_{\mathrm{OH}}r_{\mathrm{ON}}}-\frac{\cos\phi_{\mathrm{NOC}}}{r_{\mathrm{OC}}r_{\mathrm{ON}}}\right), \end{aligned} \tag{S12}$$

where m_{Acceptor} is the mass of the acceptor unit, r_{ON} is the ON bond length, ϕ_{NOH} and ϕ_{NOC} are the NOH and NOC angles, respectively. This g-matrix element is similar to that for the donor rock of the hydrated complexes in the original LMPT model,[8] with the exception that the bond length between the free H and the O atom of the donor water unit has been replaced by the OC bond length, and the mass of the free hydrogen has been replaced by the mass of the donor unit minus the mass of the OH group. The g-matrix element of the donor twist is approximated, as the sum of the inverse of the moments of inertia of two rotors around the OC bond:

$$g_{xx} = \frac{1}{m_{\mathrm{H}}\left(r_{\mathrm{OH}}\sin\phi_{\mathrm{COH}}\right)^2} + \frac{1}{\sum_i m_i\left(r_{\mathrm{C}i}\sin\phi_{\mathrm{OC}i}\right)^2}, \tag{S13}$$

where the summation in the second term is over all donor atoms except those of the COH group, m_i is the mass of atom i, $r_{\mathrm{C}i}$ is the distance between the C atom of the COH group and atom i and $\phi_{\mathrm{OC}i}$ is the OCi angle. If this approximation is used to obtain the rotational constant of the internal rotation, we get 25.49 cm^{-1}, which compares well with the experimental value of 27.63 cm^{-1}.[13]

Rayleigh-Schrödinger Perturbation theory is applied to include the effect of the two intermolecular modes on the donor vibrations. Each of the donor vibrations are coupled through the potential energy surface to each of the two intermolecular modes, where up to quartic force constants are included.[8,9] These force constants were again determined from 9×9 potential energy grids using a standard numerical technique.[8] The displacement of the OH bond was from -0.20 Å to +0.20 Å in steps of 0.05 Å, and for the other modes the displacement was from -20 degrees to +20 degrees in steps of 5 degrees. Up to fourth order corrections to the vibrational energies and first order corrections to the vibrational wavefunction were obtained.

The dimensionless oscillator strength, $f_{\mathrm{v}\leftarrow 0}$, of a transition from the vibrational ground state, ψ_0, to a vibrationally excited state, ψ_{v}, is given by the equation:[14,15]

$$f_{\mathrm{v}\leftarrow 0} = 4.702 \times 10^{-7}[\mathrm{cm\ D}^{-2}]\tilde{\nu}_{\mathrm{v}\leftarrow 0}|\vec{\mu}_{\mathrm{v}0}|^2 \tag{S14}$$

where $\tilde{\nu}_{\mathrm{v}\leftarrow 0}$ is the transition wavenumber in cm^{-1} and $\vec{\mu}_{\mathrm{v}\leftarrow 0}$ is the transition dipole moment, $\vec{\mu}_{\mathrm{v}\leftarrow 0} = \langle\psi_{\mathrm{v}}|\,\vec{\mu}\,|\psi_0\rangle$, in Debye (D). The dipole moment, $\vec{\mu}$, is expanded as a Taylor series in the two donor vibrational coordinates and the two intermolecular vibrational coordinates. Up to hextic terms in the diagonal part and quartic terms in the off-diagonal part are included.[9] The dipole moment expansion coefficients for the diagonal parts were obtained by fitting sixth order polynomials to the dipole moments calculated at the same geometries used to generate the potential energy surface. The finite field approach was used to determine the dipole moments with an applied finite field of 0.0001 a.u..[16] The dipole moment coefficients for the off-diagonal part were determined from 9×9 dipole moment grids using the same approach, which was employed to determine the expansion coefficients of the potential energy coupling.

All integrals were evaluated numerically using the trapezoidal rule and the *Matlab* software package.[17]

Table S7: Calculated frequencies (cm^{-1}) and oscillator strengths for the fundamental OH-stretching and second overtone $\mathrm{NH_f}$-stretching vibrations in the EtOH·DMA and MeOH·DMA complexes.

		OH-stretch		$\mathrm{NH_f}$-stretch	
	Method	$\tilde{\nu}$	f	$\tilde{\nu}$	f
EtOH·DMA	1D LM DFT[a]	-	2.00×10^{-4}	-	2.21×10^{-8}
	1D LM CC[b]	3258	1.66×10^{-4}	9688	1.95×10^{-8}
	LMPT CC[c]	3352	1.22×10^{-4}	9686	1.95×10^{-8}
MeOH·DMA	1D LM CC[d]	-	1.80×10^{-4}	-	1.80×10^{-8}
	1D LM CC[b]	3273	1.75×10^{-4}	9702	2.06×10^{-8}
	LMPT CC[c]	3377	1.27×10^{-4}	9700	2.07×10^{-8}

[a] Used in reference 5, assuming a Morse oscillator.[3–6,18,19]
[b] Calculated in this work using numerical integration.
[c] Calculated in this work using numerical integration.
[e] This work.
[d] Used in reference 4, assuming a Morse oscillator.[3–6,18,19] This is the value for a higher energy structure.

S5 Determined K_P values

Table S8: Equilibrium constant for the EtOH·DMA complex determined at different temperature (T in K). The average equilibrium constant from three experiments is given and so are the individual equilibrium constant from experiment 1, 2 and 3.

	K_P values			
T	average	1	2	3
RT	$19.0\pm1.9\times10^{-2}$	$21.1\times10^{-2,a}$	$17.9\times10^{-2,b}$	$18.6\times10^{-2,b}$
305	$15.3\pm1.5\times10^{-2}$	15.2×10^{-2}	15.3×10^{-2}	15.5×10^{-2}
314	$11.0\pm1.1\times10^{-2}$	11.0×10^{-2}	11.0×10^{-2}	11.0×10^{-2}
324	$7.79\pm0.8\times10^{-2}$	7.52×10^{-2}	7.93×10^{-2}	7.96×10^{-2}
334	$5.76\pm0.6\times10^{-2}$	5.60×10^{-2}	5.57×10^{-2}	6.21×10^{-2}
344	$4.09\pm0.4\times10^{-2}$	4.00×10^{-2}	3.93×10^{-2}	4.39×10^{-2}
354	$3.08\pm0.3\times10^{-2}$	2.99×10^{-2}	3.13×10^{-2}	3.13×10^{-2}
364	$2.27\pm0.2\times10^{-2}$	2.11×10^{-2}	2.32×10^{-2}	2.41×10^{-2}
374	$1.49\pm0.1\times10^{-2}$	1.27×10^{-2}	1.69×10^{-2}	1.67×10^{-2}

a: At 301 K.
b: At 303 K.

Table S9: Equilibrium constant for the MeOH·DMA complex determined at different temperature (T in K). The average equilibrium constant from three experiments is given and so are the individual equilibrium constant from experiment 4 and 5.

	K_P values		
T	average	4	5
RT	$21.2 \pm 2.6 \times 10^{-2}$	$25.5 \times 10^{-2,a}$	$18.9 \times 10^{-2,b}$
305	$17.2 \pm 2.1 \times 10^{-2}$	18.7×10^{-2}	16.1×10^{-2}
314	$12.7 \pm 1.5 \times 10^{-2}$	14.4×10^{-2}	11.6×10^{-2}
324	$9.55 \pm 1.2 \times 10^{-2}$	10.6×10^{-2}	8.79×10^{-2}
334	$7.12 \pm 0.9 \times 10^{-2}$	8.23×10^{-2}	6.44×10^{-2}
344	$5.23 \pm 0.6 \times 10^{-2}$	5.91×10^{-2}	4.79×10^{-2}
354	$3.99 \pm 0.5 \times 10^{-2}$	4.48×10^{-2}	3.67×10^{-2}
364	$2.91 \pm 0.4 \times 10^{-2}$	3.34×10^{-2}	2.63×10^{-2}
374	$1.72 \pm 0.2 \times 10^{-2}$	2.23×10^{-2}	1.49×10^{-2}

a: At 301 K.
b: At 299 K.

S6 Determined ΔH values

In Figure S12, lnK_P is plotted as a function of T^{-1}. Straight lines are fitted to the data points and ΔH values are obtained for the individual experiments, 1 - 5. In Figure S13, lnK_P is plotted as a function of T^{-1}, as in Figure S12; however, the room temperature data have been included.

In Figure S14, a straight line is fitted to the data, and average ΔH values of -31.5 kJ/mol and -29.4 kJ/mol are obtained for the EtOH·DMA and MeOH·DME complex, respectively.

In Figure S15, we divided our data into two ranges, 305 - 334 K and 344 - 374 K. However, due to the small number of data points in each range, the standard error of the individual fits is larger than the difference in the ΔH values, and a temperature dependence of ΔH could not be concluded.

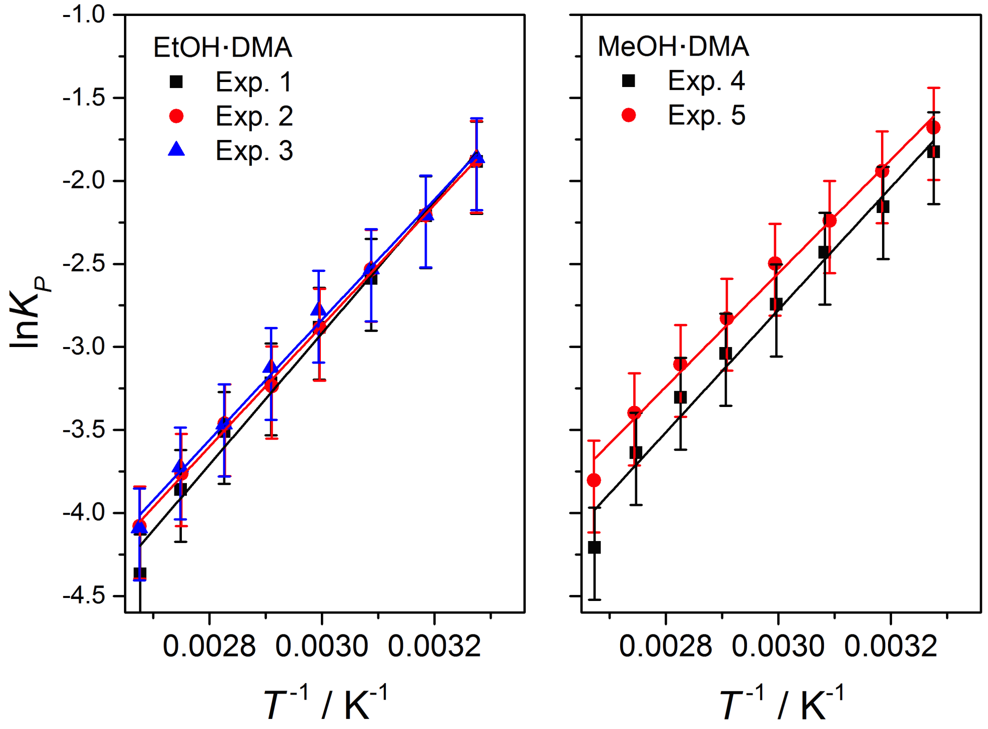

Figure S12: The $\ln K_P$ *versus* T^{-1} plot for the EtOH·DMA (experiments 1, 2, and 3) and MeOH·DMA complexes (experiments 4 and 5) The slope of the fits are -$\Delta H/R$. The room temperature measurement is excluded and -$\Delta H/R$ values of 3956±428 K^{-1}, 3644±428 K^{-1} and 3626±427 K^{-1} are obtained for the EtOH·DMA complex experiments 1, 2, and 3, respectively. -$\Delta H/R$ values of 3689±425 K^{-1} and 3420±424 K^{-1} are obtained for the MeOH·DMA complex experiments 4 and 5, respectively.

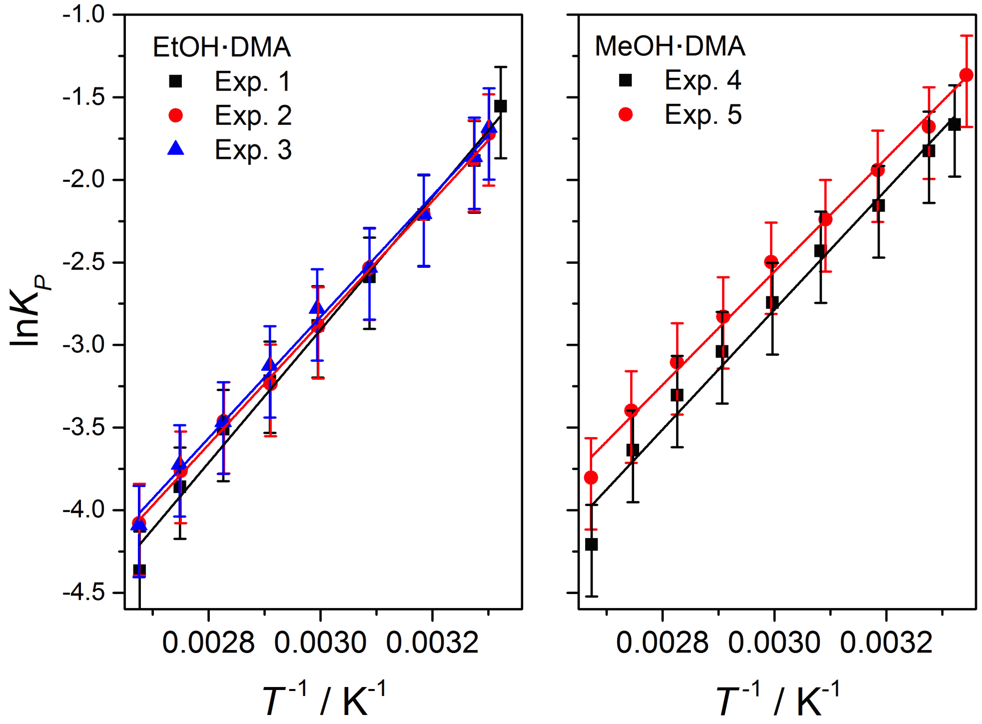

Figure S13: The lnK_P *versus* T^{-1} plot for the EtOH·DMA (experiments 1, 2, and 3) and MeOH·DMA complexes (experiments 4 and 5). The slope of the fits are -$\Delta H/R$. The room temperature measurement is included and -$\Delta H/R$ values of 4023±366 K^{-1}, 3685±372 K^{-1} and 3670±371 K^{-1} are obtained for the EtOH·DMA complex experiments 1, 2, and 3, respectively. -$\Delta H/R$ values of 3632±364 K^{-1} and 3433±357 K^{-1} are obtained for the MeOH·DMA complex experiments 4 and 5, respectively.

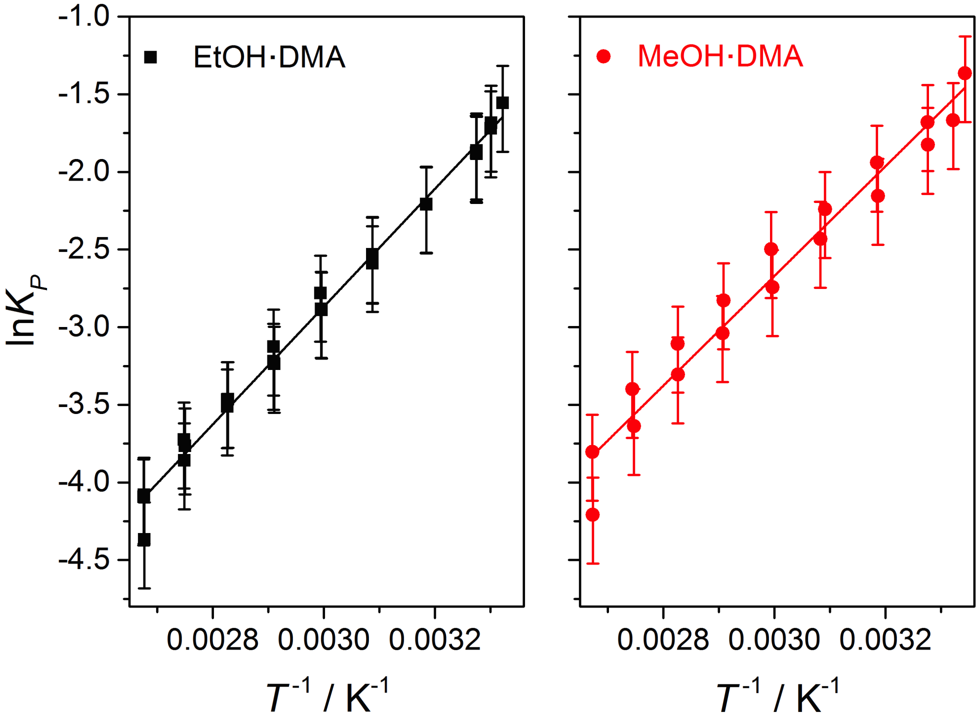

Figure S14: The $\ln K_P$ *versus* T^{-1} plot for the EtOH·DMA (black squares) and MeOH·DMA (red circles) complexes, where the room temperature measurement is included. The slope of the fit is $-\Delta H/R$, which is 3794±213 K^{-1} and 3534±255 K^{-1} for the EtOH·DMA and MeOH·DMA complexes, respectively.

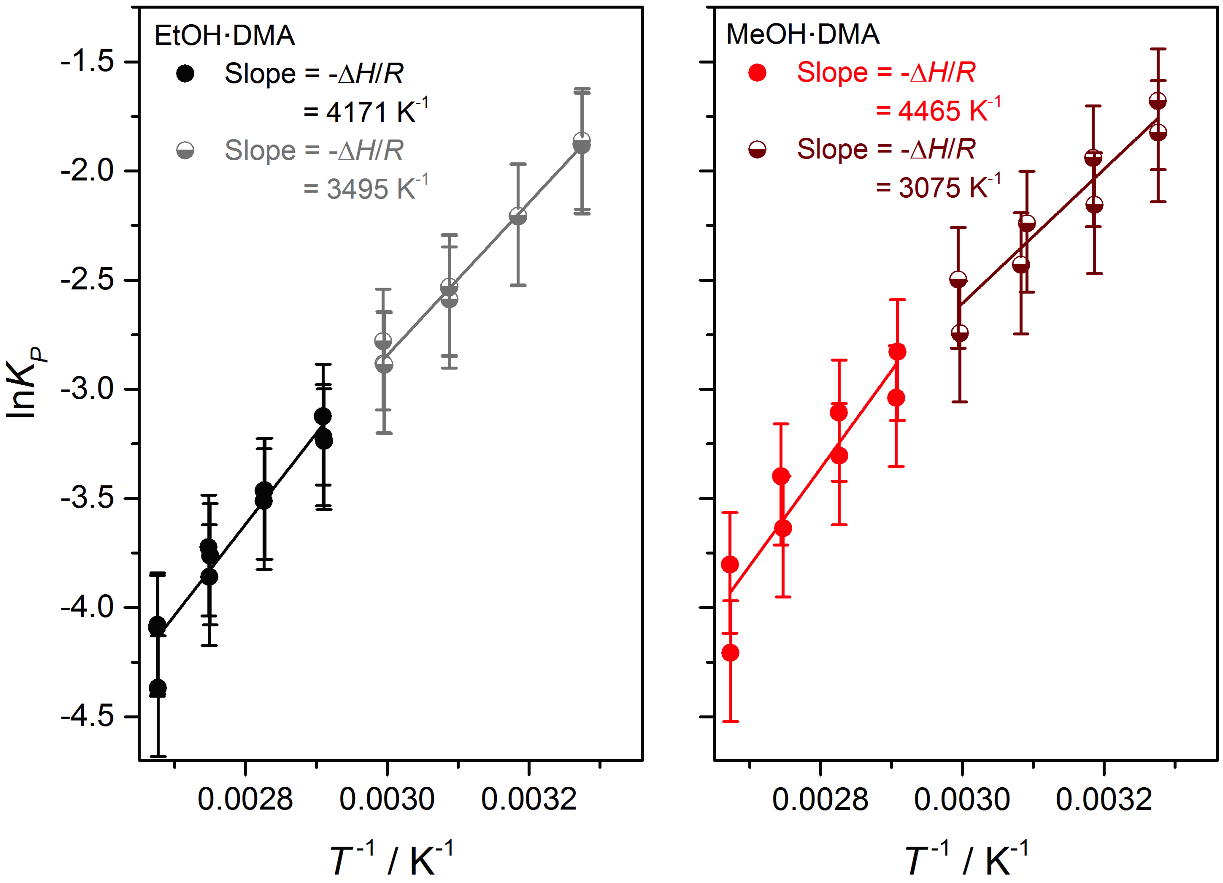

Figure S15: The $\ln K_P$ *versus* T^{-1} plot for the EtOH·DMA and MeOH·DMA complexes, where our data is divided into two ranges. The room temperature data have been excluded in the fits. The slope of the fits are -$\Delta H/R$, which is 4171±792 K^{-1} and 3495±660 K^{-1} for the EtOH·DMA complex and 4465±962 K^{-1} and 3075±804 K^{-1} MeOH·DMA complexes, respectively.

The maximum absorbance (A_{max}) is also a measure for the band intensity like the integrated absorbance. We determine ΔH using A_{max} according to the equations given in Section S2. The use of A_{max} does assume that the band shape does not change with temperature, but does provide a useful check on the integration. In Figures S16 and S17, $\ln(TA_{\text{max}}/(P_{\text{A}}/P^{\ominus}P_{\text{B}}/P^{\ominus}))$ is plotted against T^{-1} without and with the room temperature data, respectively.

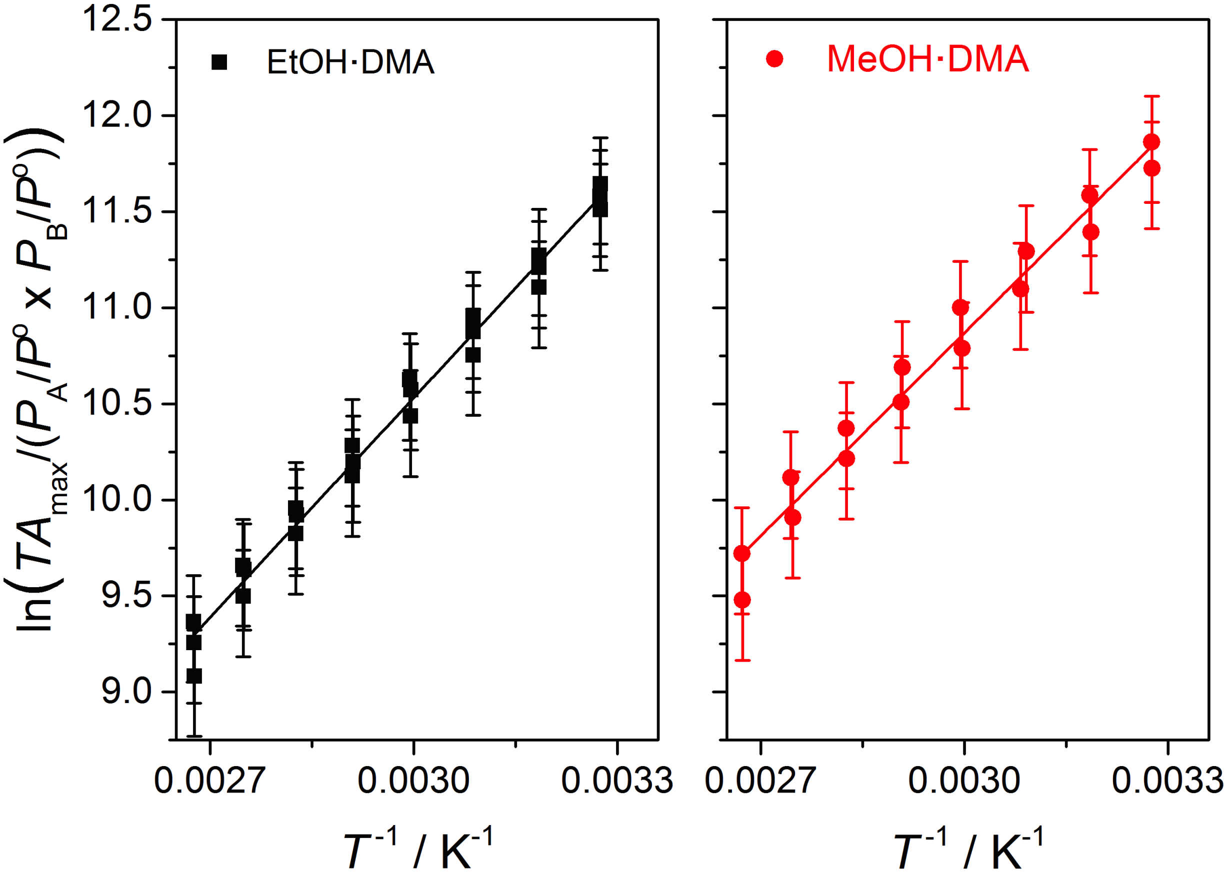

Figure S16: The $\ln(TA_{\text{max}}/(P_{\text{A}}/P^{\ominus}P_{\text{B}}/P^{\ominus}))$ *versus* T^{-1} plot for the EtOH·DMA and MeOH·DMA complexes. The room temperature data have been excluded. The slope of the fit is -$\Delta H/R$, which is 3810±247 K^{-1} and 3519±300 K^{-1} for the EtOH·DMA and MeOH·DMA complexes, respectively.

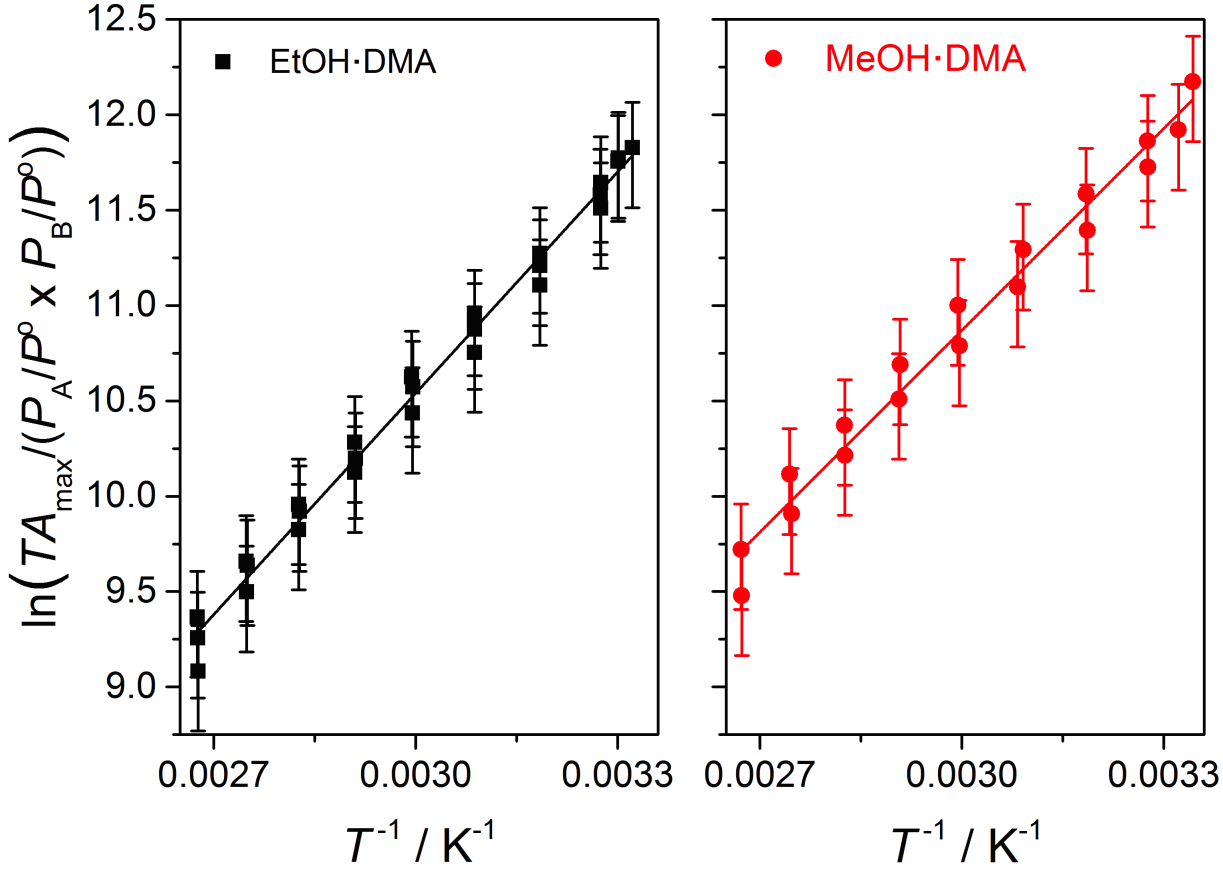

Figure S17: The $\ln(TA_{\mathrm{max}}/(P_{\mathrm{A}}/P^{\ominus}P_{\mathrm{B}}/P^{\ominus}))$ *versus* T^{-1} plot for the EtOH·DMA and MeOH·DMA complexes where the RT measurement is included. The slope of the fit is -$\Delta H/R$, which is 3869±213 K^{-1} and 3528±255 K^{-1} for the EtOH·DMA and MeOH·DMA complexes, respectively.

Table S10: Determined ΔH (kJ/mol) values from the individual experiments of the EtOH·DMA and MeOH·DMA complexes, with (+RT) and without (÷RT) the room temperature measurements. Values based on the integrated absorbance and the maximum absorbance are given.

		$-\Delta H$ values EtOH·DMA				$-\Delta H$ values MeOH·DMA		
		average	1	2	3	average	4	5
Int. Abs.	÷RT	31.1±2	32.9±4	30.3±4	30.1±4	29.5±2	30.7±4	28.4±4
	+RT	31.5±2	33.4±3	30.6±	30.5±3	29.4±2	30.2±3	28.5±3
A_{max}	÷RT	31.7±2	-	-	-	29.3±2	-	-
	+RT	32.3±2	-	-	-	29.3±2	-	-

S7 Previous temperature investigations

S7.1 The MeOH·DMA complex

Temperature experiments of the MeOH·DME, MeOH·DMS, MeOH·DMA, MeOH·TMA and $(\mathrm{DMA})_2$ complexes have previously been performed.[4,18,20] In these studies, the product of the monomer pressures, $P_\mathrm{A}P_B$, was kept constant at all temperatures. Initially, a room temperature spectrum was measured of a sample. The cell was then connected to the vacuum line and emptied. To ensure that the pressure at the elevated temperatures was the same as that in the initial room temperature measurement, the amount of sample pressure to be transferred into the cell at room temperature was reduced as calculated from the ideal gas law. The sample was then transferred to the cell, and the cell was then heated. If the $P_\mathrm{A}P_\mathrm{B}$ product is kept fixed, K_P is directly proportional to P_AB, hence K_P is directly proportional to the temperature times the integrated absorbance ($T\int A(\tilde{\nu})\mathrm{d}\tilde{\nu}$), see equations S4 - S7. However in the previous work, $\ln(\int A(\tilde{\nu})\mathrm{d}\tilde{\nu})$ was plotted against T^{-1}, from which ΔH was determined. The temperature was left out, which makes a small change in the determined ΔH values. We have taken the original data for the MeOH·DMA and MeOH·TMA complexes[4] and replotted it as $\ln(T\int A(\tilde{\nu})\mathrm{d}\tilde{\nu})$ versus T^{-1}. In Figure S18, the new linear fits are shown, from which ΔH values are determined from the linear fit.

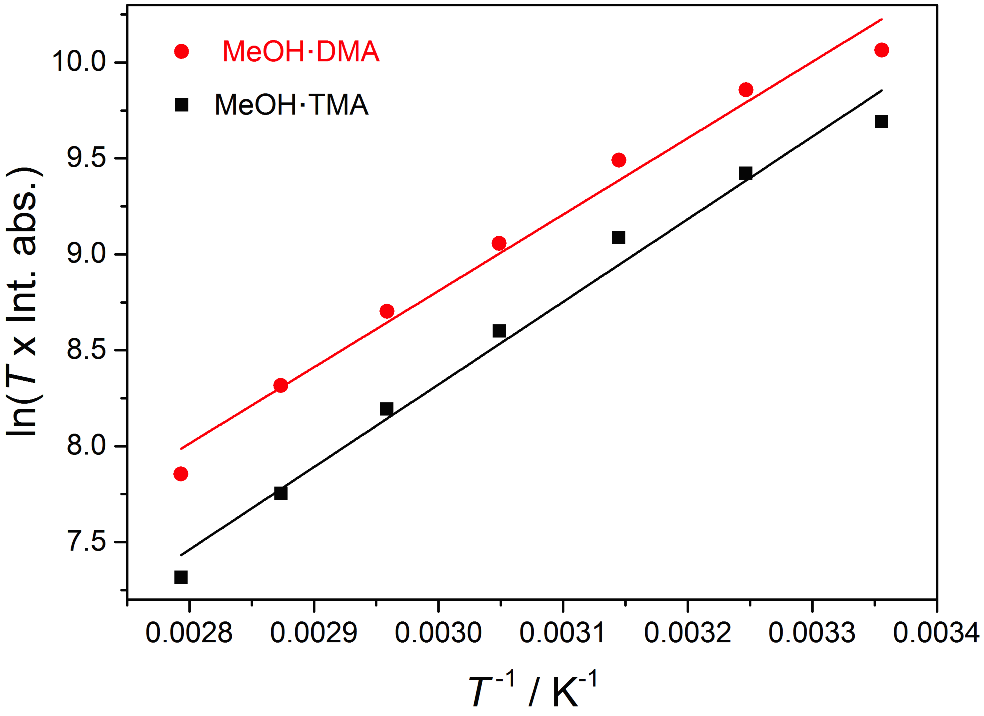

Figure S18: The $\ln(T \int A(\tilde{\nu})\mathrm{d}\tilde{\nu})$ plotted against T^{-1} for the MeOH·DMA (red circles) and MeOH·TMA (black squares) complexes. The slope of the fit is $-\Delta H/R$, which is 3981 K^{-1} and 4308 K^{-1} for the MeOH·DMA and MeOH·TMA complexes, respectively. ΔH values of -33.1 kJ/mol and -35.8 kJ/mol are obtained for the MeOH·DMA and MeOH·TMA complexes, respectively. If the room temperature measurements ($T^{-1} = 0.00335\ \mathrm{K}^{-1}$) are removed from the fit ΔH values of -36.3 kJ/mol and -39.1 kJ/mol are obtained for the MeOH·DMA and MeOH·TMA complexes, respectively.

We obtain ΔH values of -33.1 kJ/mol and -35.8 kJ/mol for the MeOH·DMA and MeOH·TMA complexes, respectively, compared to the values of -35.8 kJ/mol and -38.2 kJ/mol, respectively.[4] In the $\ln \int A(\tilde{\nu})\mathrm{d}\tilde{\nu}$ versus T^{-1} plot, a curvature as a function of temperature was observed, and ΔH was concluded to be temperature dependent.[4] A curvature as a function of temperature is also observed in the corrected data in Figure S18. The deviations from a linear correlation may arise from experimental uncertainties related to the pressure determination with the ideal gas law, as discussed previously, and the assumption of a fixed $P_\mathrm{A}P_\mathrm{B}$ product may be more uncertain. We expect the uncertainties given in these previous studies to be larger than given.[4,21,22]

S7.2 The EtOH·DMA complex

We have taken the experimental data previously recorded of the EtOH·DMA complex,[5] and re-integrated the fundamental OH-stretching and second overtone NH_f-stretching vibrations. In Figure S19, we compare integrations of the OH-stretching band previously performed (a) and recently performed (b). In both integrations a straight baseline was drawn between two points on either side of the observed band. In the previous integration, Lorentzian functions were fitted to the observed band, from which the integrated absorbance was obtained.[5] In the new integration, the integrated absorbance was simply obtained by the area of the enclosure, as shown in part (b) of the figure. We believe, that the new integration is more accurate than that previously performed. In Table S11, we summarise the integrated absorbance of the OH- and NH_f-stretching bands, with a difference of about 20 %.

In reference 5, a 50%/50% average of the local mode B3LYP/aug-cc-pVTZ calculated oscillator strengths was used to determine the pressure of the complex (P_{AB}), and hence the K_P value. We have re-calculated P_{AB} and K_P using only the oscillator strength of the lowest energy conformer. In Table S12, the calculated oscillator strengths are given. In the previous study of the second overtone of NH_f-stretching vibration in EtOH·DMA complex, the M06-2X/aug-cc-pVTZ oscillator strength was accidently used to determine P_{AB}, even though it was stated that the B3LYP/aug-cc-pVTZ oscillator strength was used. The 1.34×10^{-8} value given in Table S12, is the 50%/50% average M06-2X/aug-cc-pVTZ oscillator strength of the second overtone NH_f-stretching vibration used in reference 5. In Table S12, we also give the K_P and ΔG values determined from the 1D local mode B3LYP/aug-cc-pVTZ calculated oscillator strengths.

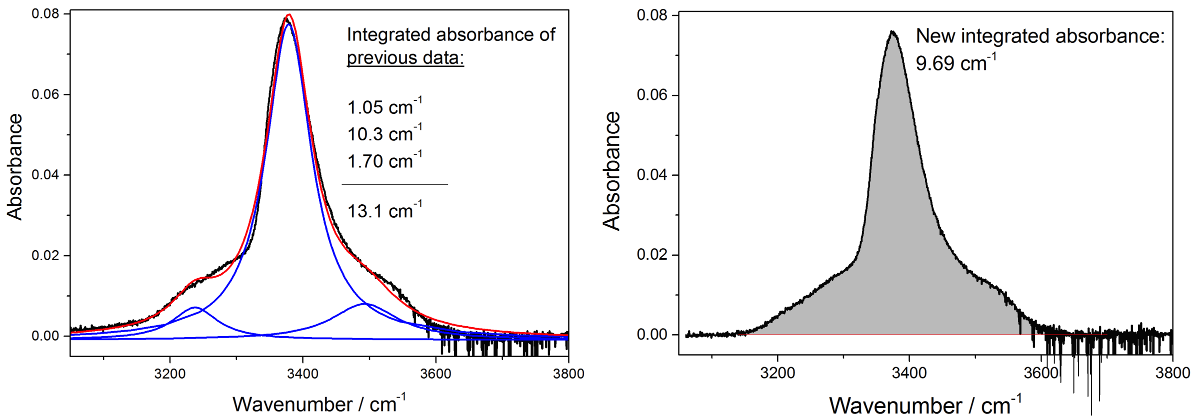

(a) (b)

Figure S19: The integrated absorbance of the OH-stretching band in the EtOH·DMA complex. (a) The integration previously performed in reference 5. (b) New improved integration of the data from reference 5.

Table S11: Integrated absorbance (cm^{-1}) of the fundamental OH-stretching and second overtone NH$_f$-stretching vibrations in the EtOH·DMA complex. For the new data the integration ranges were 3148 - 3700 cm^{-1} and 9500 - 9750 cm^{-1} for the OH- and NH$_f$-stretching vibrations.

OH-stretch		NH$_f$-stretch	
Previous data[a]	New data	Previous data[a]	New data
15.2	13.2	0.20	0.16
13.1	9.69	0.14	0.11
11.7	8.99	-	-
11.4	8.97	-	-
7.81	6.05	-	-
6.19	4.91	-	-

a: Reference 5.

Table S12: Calculated one dimensional local mode oscillator strengths of the fundamental OH-stretching and second overtone NH_f-stretching vibrations in the EtOH·DMA complex. The determined K_P values and ΔG values (kJ/mol) are also given.

	OH-stretch		NH_f-stretch	
	Previous data[a]	New data	Previous data[a]	New data
f	2.17×10^{-4},[b]	2.00×10^{-4},[b]	1.34×10^{-8},[c]	2.21×10^{-8},[b]
K_P	0.11	0.092	0.44	0.21
ΔG	5.47	5.90	2.03	3.85

a: Reference 5.

b: Calculated with the B3LYP/aug-cc-pVTZ method and 1D LM assuming a Morse oscillator.[3–6,18,19]

c: Calculated with the M06-2X/aug-cc-pVTZ method and 1D LM assuming a Morse oscillator.

References

(1) Chung, S.; Hippler, M. *J. Chem. Phys.* **2006**, *124*, 214316.

(2) Hippler, M. *J. Chem. Phys.* **2007**, *127*, 084306.

(3) Du, L.; Lane, J. R.; Kjaergaard, H. G. *J. Chem. Phys.* **2012**, *136*, 184305.

(4) Du, L.; Mackeprang, K.; Kjaergaard, H. G. *Phys. Chem. Chem. Phys.* **2013**, *15*, 10194–10206.

(5) Hansen, A. S.; Du, L.; Kjaergaard, H. G. *Phys. Chem. Chem. Phys.* **2014**, *16*, 22882–22891.

(6) Andersen, C. L.; Jensen, C. S.; Mackeprang, K.; Du, L.; Jørgensen, S.; Kjaergaard, H. G. *J. Phys. Chem. A* **2014**, *118*, 11074–11082.

(7) Hansen, A. S.; Du, L.; Kjaergaard, H. G. *J. Phys. Chem. Lett.* **2014**, *5*, 4225–4231.

(8) Mackeprang, K.; Kjaergaard, H. G.; Salmi, T.; Hänninen, V.; Halonen, L. *J. Chem. Phys.* **2014**, *140*, 184309.

(9) Mackeprang, K.; Hänninen, V.; Halonen, L.; Kjaergaard, H. G. *J. Chem. Phys.* **2015**, *142*, 094304.

(10) Kjaergaard, H. G.; Henry, B. R.; Wei, H.; Lefebvre, S.; Carrington, T.; Mortensen, O. S.; Sage, M. L. *J. Chem. Phys.* **1994**, *100*, 6228–6239.

(11) Wilson, E. B.; Decius, J. C.; Cross, P. C. *Molecular Vibrations*; Dover: New York, 1980.

(12) Meyer, R. *J. Chem. Phys.* **1970**, *52*, 2053–2059.

(13) Pei, C. C.; Gou, Q. Q.; Zeng, Q. *Astron. Astrophys. Suppl. Ser.* **1988**, *76*, 35–52.

(14) Atkins, P.; Friedman, R. *Molecular Quantum Mechanics*; Oxford University Press: London, 2005.

(15) Kjaergaard, H. G.; Yu, H.; Schattka, B. J.; Henry, B. R.; Tarr, A. W. *J. Chem. Phys.* **1990**, *93*, 6239–6248.

(16) Miller, B. J.; Lane, J. R.; Kjaergaard, H. G. *Phys. Chem. Chem. Phys.* **2011**, *13*, 14183–14193.

(17) *MATLAB and Statistics Toolbox Release R2013a*; The MathWorks Inc.: Natick, Massachusetts, United States.

(18) Du, L.; Kjaergaard, H. G. *J. Phys. Chem. A* **2011**, *115*, 12097–12104.

(19) Mackeprang, K.; Schrøder, S. D.; Kjaergaard, H. G. *Chem. Phys. Lett.* **2013**, *582*, 31–37.

(20) Howard, D. L.; Kjaergaard, H. G. *Phys. Chem. Chem. Phys.* **2008**, *10*, 4113–4118.

(21) Fild, M.; Swiniarski, M. F.; Holmes, R. R. *Inorg. Chem.* **1970**, *9*, 839–843.

(22) Millen, D. J.; Mines, G. W. *J. Chem. Soc., Faraday Trans. 2* **1974**, *70*, 693–699.